





The Transformation of Centaurs into Jupiter-family Comets

Jeremy Wood^{1,2}  and Tobias C. Hinse^{3,4} ¹ American Military University, 111 W. Congress Street, Charles Town, WV 25414, USA² University of Southern Queensland, Computational Engineering and Science Research Centre, West St, Toowoomba, QLD 4350, Australia³ Institute of Astronomy, Faculty of Physics, Astronomy and Informatics, Nicolaus Copernicus University, Grudziadzka 5, 87-100 Torun, Poland; tchinse@gmail.com⁴ Chungnam National University, Department of Astronomy and Space Science, 34134 Daejeon, Republic of Korea

Received 2021 June 16; revised 2022 February 24; accepted 2022 February 27; published 2022 April 25

Abstract

Centaurs are an ephemeral class of objects that can evolve into Jupiter-family comets (or JFCs) due to gravitational perturbations from the giant planets. In this work, we use numerical integration of massless test particles in the six-body problem (the Sun, four giant planets, and a test particle) to study the transformation of Centaurs into JFCs. We find that Centaurs can transform into JFCs via a rapid, continuous drop in perihelion or aphelion distance to a value below 5.2 au or 7 au, respectively, typically within 5 yr from the start of the drop. We call these JFC perihelion drops and JFC aphelion drops, respectively. These drops are correlated with close approaches to Jupiter. For such perihelion and aphelion drops, the maximum possible fractional change in the associated perihelion or aphelion distance increases with decreasing close-approach distance to Jupiter. A perihelion barrier may exist at 6.3 au. If so, then it must be crossed from above in order for a Centaur to transform into a JFC due to a single close approach to Jupiter. Currently, 93 (or 11%) of the known Centaurs have a perihelion distance, q , below 6.3 au. If the inclination of the orbit of the Centaur to the ecliptic plane is above 10° , then orbits with $q > 6.3$ au and $2 < T_J < 3$ can exist, where T_J is the Tisserand parameter with respect to Jupiter. Small bodies in such orbits could be classified as either Centaurs or JFCs.

Unified Astronomy Thesaurus concepts: [Short period comets \(1452\)](#); [Comet dynamics \(2213\)](#); [Centaur group \(215\)](#); [Comets \(280\)](#); [Small Solar System bodies \(1469\)](#)

1. Introduction

It is known that small solar system bodies (SSSBs) can evolve into Jupiter-family comets (JFCs) from orbits interior to Jupiter (Hsieh et al. 2020) and from the Centaur region from orbits exterior to Jupiter (Grazier et al. 2019; Roberts & Muñoz-Gutiérrez 2021).

Centaurs are an ephemeral population of icy SSSBs with orbits among the giant planets. There is no universally accepted definition of a Centaur. For example, the Minor Planet Center (MPC) defines Centaurs as SSSBs with perihelion distances and semimajor axes between the orbits of Jupiter (5.2 au) and Neptune (30.1 au) that are not co-orbitals or satellites (Tiscareno & Malhotra 2003; Di Sisto & Brunini 2007),⁵ while the Jet Propulsion Laboratory defines Centaurs as SSSBs with semimajor axes, a , in the range $5.5 \text{ au} < a < 30.1 \text{ au}$ with no restriction on perihelion distance.

Using these definitions yields a current Centaur population of 815 and 702, respectively. In this work, we adopt the MPC definition of Centaur. The orbits of these bodies are typically highly chaotic and unstable due to frequent close approaches to the four giant planets (Horner et al. 2004a; Bailey & Malhotra 2009). The average dynamical lifetime of a Centaur is approximately 10 Myr (Levison & Duncan 1994; Dones et al. 1996; Tiscareno & Malhotra 2003; Duncan et al. 2004). Since this amount of time is far less than the age of the solar

system (4.6 Gyr), it is believed that Centaurs originated elsewhere.

The prevailing theory is that most Centaurs originated in the trans-Neptunian region (Levison & Duncan 1997; Emel'yanenko et al. 2005; Di Sisto & Brunini 2007; Volk & Malhotra 2008; Marsden 2009; Brassier et al. 2012; de la Fuente Marcos & de la Fuente Marcos 2014; Fouchard et al. 2014), though other source populations have been proposed such as the Jupiter Trojans (Horner et al. 2004b; Horner & Wyn Evans 2006; Horner et al. 2012) and the Neptune Trojans (Horner & Lykawka 2010; Lykawka & Horner 2010; Horner et al. 2012; Peixinho et al. 2020).

As the orbits of Centaurs are perturbed by the gravitational forces of the giant planets, they may eventually collide with the Sun, collide with a planet, be captured as temporary satellites of the Jovian planets, or evolve into other classes of objects such as Trojans, trans-Neptunian objects (TNOs), or the previously mentioned JFCs (Tiscareno & Malhotra 2003; Horner et al. 2004a, 2004b; Grazier et al. 2019; Roberts & Muñoz-Gutiérrez 2021).

It is known that a Centaur can transform into a JFC via a close approach to a giant planet that decreases the perihelion distance, q , until the orbit becomes cometary (Horner et al. 2004a). Close approaches to Jupiter in particular are involved in the transformation of Centaurs into JFCs (Horner & Jones 2009; Grazier 2016; Grazier et al. 2019).

But since there is no universally accepted definition of a JFC, the exact point in time at which a body transforms into a JFC can be debatable. JFCs are loosely defined as short-period comets with orbital periods < 20 yr whose dynamics are mainly controlled by Jupiter (Levison & Duncan 1997; Marsden 2009). Levison (1996) defines JFCs as small bodies with a Tisserand parameter with respect to Jupiter, T_J , in the range $2 < T_J < 3$. T_J

⁵ <http://minorplanetcenter.net/iau/lists/Unusual.html> (Accessed: 2022 Jan. 8).

is defined as

$$T_J = \frac{a_J}{a} + 2 \cos(i - i_J) \sqrt{\frac{a}{a_J}(1 - e^2)}, \quad (1)$$

where a_J , i_J , e , and i are the semimajor axis ($a_J = 5.2$ au) and inclination ($i_J = 1^\circ.3$ with respect to the ecliptic plane) of the orbit of Jupiter, and the eccentricity and inclination with respect to the ecliptic plane of the small body's orbit, respectively.

Equation (1) can be rewritten in terms of the perihelion distance, q , and the aphelion distance, Q , defined by

$$q = a(1 - e), \quad (2)$$

$$Q = a(1 + e). \quad (3)$$

The result is

$$T_J = 2 \frac{a_J}{q + Q} - 2 \cos(i - i_J) \sqrt{\frac{2qQ}{a_J(q + Q)}}. \quad (4)$$

Di Sisto et al. (2019) define JFCs as small bodies with orbital periods < 20 yr and $2 < T_J < 3.15$, while Sarid et al. (2019) define JFCs as a population of small bodies with $2 < T_J < 3$, $q < a_J$, and $Q < 7$ au. The latter restriction is applied in order to select those bodies that are well separated from Saturn. This is the so-called q-Q definition that we will adopt in this work. Applying the q-Q definition to the JPL Small-Body Database⁶ yields a total JFC population of 441.

The purpose of this work is to study the transformation of Centaurs into JFCs according to the q-Q definition using numerical integration of massless test particles. One reason why it is important to study the mechanisms by which Centaurs transform into JFCs is because if a large Centaur was to make its way into the inner solar system, it could threaten Earth with a direct impact (Grazier 2016) or spread large amounts of debris that could block sunlight from reaching Earth (Hahn & Bailey 1990).

JFCs themselves are also important objects of study because they can still contain within them undisturbed material from the original solar nebula that formed the solar system, despite internal heating disturbing some of this original material (Gkotsinas et al. 2022). By studying this pristine material, we learn more about the formation of the solar system and the composition of objects in the outer solar system without having to go there (Jehin et al. 2006; Stodolna et al. 2014).

This paper is structured as follows. Section 1 introduces the topic, Section 2 details our experimental method of integration, Section 3 presents our results, and we summarize our conclusions in Section 4.

2. Method

A total of 22,625 massless test particles initially in a region of $a - e$ space where $q > 5.4$ au and $Q < 7.8$ au were integrated for 10^5 yr in a fully interacting six-body problem (the Sun, four giant planets, and a test particle). This region and integration time were chosen only because it is known that typically it takes $< 10^5$ yr for a Centaur in this region to evolve into a JFC (Sarid et al. 2019; Roberts & Muñoz-Gutiérrez 2021). Any other significance of this particular region of $a - e$ space is outside the scope of this work. The masses of the inner planets were added to the Sun as their effect on the dynamics of

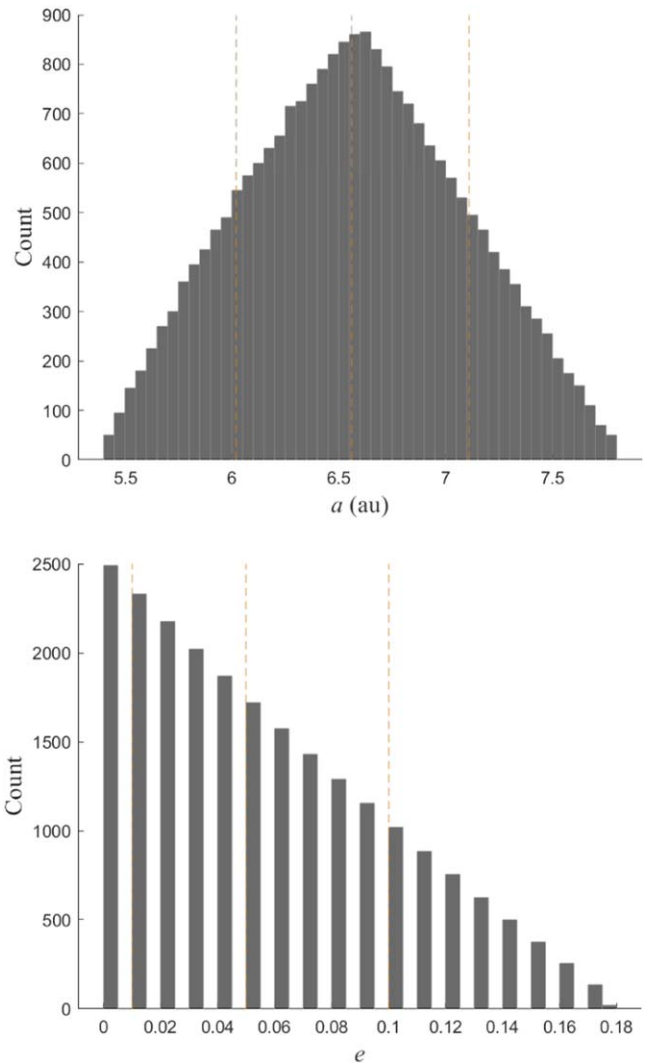


Figure 1. Histograms of the semimajor axes (top panel) and eccentricities (bottom panel) of the initial orbits of 22,625 test particles. The three dashed lines in each panel represent the 16th percentile, the median, and the 84th percentile, from left to right. The bin sizes of the top and bottom panels are 0.05 au and 0.005, respectively.

Centaurs is not significant (Horner et al. 2004a, 2004b; Grazier et al. 2019).

To determine the initial semimajor axis and eccentricity of each test particle, 500 evenly spaced contours of constant perihelion distance were sampled in $a - e$ space in the range $5.4 \text{ au} < q < 7.8 \text{ au}$. In $a - e$ space, each contour extended from the line defined by $e = 0$ to the contour $Q = 7.8$ au. Test particles were distributed along each contour so that each consecutive test particle on a contour was separated from its closest neighbor(s) by a change in eccentricity of 0.01. Given that $e < 1$ for elliptical orbits, 0.01 is a natural selection for this eccentricity difference as it is two orders of magnitude below 1. This yielded a total of 4525 unique $a - e$ pairs.

Figure 1 shows histograms of the initial semimajor axes (top panel) and eccentricities (bottom panel) of the orbits of our test particles. Bin sizes are 0.05 au and 0.005, respectively. Bin sizes for these and other histograms in this work were computed using MATLAB (MATLAB 2018). We used the basic histogram(X) function in MATLAB, which creates a histogram plot of X. This function uses a built-in algorithm that

⁶ https://ssd.jpl.nasa.gov/tools/sbdb_query.html (Accessed: 2022 Jan. 9).

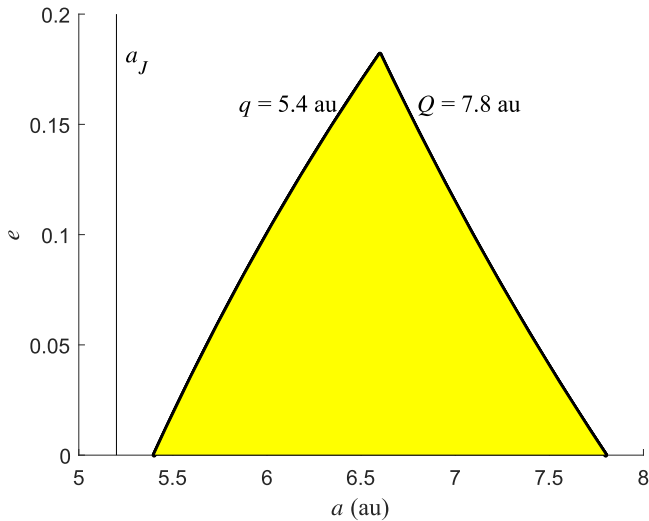


Figure 2. The perihelion distance contour of $q = 5.4$ au in $a - e$ space terminating on the $Q = 7.8$ au contour. Test particles were originally placed in the shaded region between these two contours. a_J represents the semimajor axis of Jupiter at 5.2 au.

returns bins with a uniform width, chosen to cover the range of elements in X and reveal the underlying shape of the distribution. The height of each bin represents the quantity contained in the bin.⁷ Figure 2 shows the perihelion distance contour of $q = 5.4$ au in $a - e$ space terminating on the $Q = 7.8$ au contour. Test particles were originally placed in the shaded region between these two contours.

The initial inclination and longitude of the ascending node of the orbit of each test particle were set to that of Jupiter’s orbit. This forced the orbit of each test particle to be coplanar with Jupiter’s orbit. This was done in order to maximize the initial perturbing gravitational force on q due to Jupiter as only planar forces can perturb q (Murray & Dermott 1999).

The initial argument of perihelion of each test particle, ω , was set to π radians ahead of the argument of perihelion of Jupiter’s orbit, ω_J , using

$$\omega = \omega_J + \pi. \quad (5)$$

This was done so that the aphelion of Jupiter’s orbit would be colinear with the perihelion of the orbit of the test particle and the Sun on the same side of the Sun, minimizing the initial minimum orbital intersection distance (MOID) to help facilitate close encounters (Wiżniowski & Rickman 2013).

Then for each $a - e$ pair, five test particle clones were created using the following five equally spaced values of mean anomaly: 0° , 72° , 144° , 216° , and 288° .

The total number of test particles was then $4525 \times 5 = 22,625$. There is nothing particularly significant about our selected number of test particles except that it is close to twice the number of test particles observed by Sarid et al. (2019) to pass through this region of $a - e$ space in their study.

The initial orbital parameters of the planets were found using the ephemeris service provided by Park et al. (2021)⁸ for the epoch 2000 January 1 at 0:00 UT. This date holds no special significance but has been used in previous work (Wood et al. 2017, 2018a).

The IAS15 integrator in the REBOUND N -body simulation package (Rein & Liu 2012; Rein & Spiegel 2015) was used for all integrations. This is a high-accuracy, nonsymplectic integrator with adaptive timestepping. Test particles and planets moved only due to the influence of the gravitational forces of the Sun and the four giant planets. Nongravitational forces due to collisions, fragmentation, and cometary activity were not considered in this work, though some Centaurs have been known to display cometary activity at distances beyond the orbit of Jupiter (Jewitt 2009) and activity can effect the dynamical behavior of Centaurs (Fernández et al. 2018).

To determine an appropriate output time, we analytically analyzed close approaches of test particles to Jupiter on hyperbolic trajectories relative to Jupiter. Close-approach distances to Jupiter associated with such trajectories were measured in terms of Jupiter Hill radii and labeled d_J . To compute the Hill radius of Jupiter and that of the other giant planets, we used the standard formula for Hill radius of a planet for elliptical orbits with low eccentricity given by

$$r_H = a_p \left(\frac{M_p}{3M_{\text{Sun}}} \right)^{\frac{1}{3}} \quad (6)$$

(Wood 2019), where r_H is the Hill radius of the planet, a_p is the semimajor axis of the heliocentric orbit of the planet, M_p is the mass of the planet, and M_{Sun} is the mass of the Sun.

Using this formula, we found the Hill radii of Jupiter, Saturn, Uranus, and Neptune to be $r_{\text{JH}} = 0.355$ au, $r_{\text{SH}} = 0.438$ au, $r_{\text{UH}} = 0.469$ au, and $r_{\text{NH}} = 0.776$ au, respectively. For the trajectories we studied, we used close-approach distances of one physical radius of Jupiter ($0.00135r_{\text{JH}}$), $0.01r_{\text{JH}}$, and $0.1r_{\text{JH}}$. We used a range of 1 km s^{-1} – 10 km s^{-1} for integer velocities at infinity, v_∞ , for these hyperbolic trajectories. This range is typical for Centaurs that have close approaches to Jupiter (Wood et al. 2018b). A hyperbolic trajectory could be used to study these close approaches since each small body would be well within Jupiter’s sphere of influence of about $0.9r_{\text{JH}}$ (Sellers et al. 2005).

The maximum error in the close-approach distance due solely to the output time was found by finding the difference between the radial distance to Jupiter at half an output time after perijove and the radial distance to Jupiter at perijove. Output times of 0.01 yr, 0.25 yr, 0.50 yr, 0.75 yr, and 1 yr were examined. We found that for the most extreme encounter at one Jupiter radius with $v_\infty = 10 \text{ km s}^{-1}$ with a step time of 0.01 yr, the maximum error was $0.05r_{\text{JH}}$ (or 0.02 au), which is less than one-tenth the semimajor axis of the orbit of Mercury. At a close-approach distance of $0.1r_{\text{JH}}$, the maximum error dropped to $0.005r_{\text{JH}}$ (or 0.002 au).

As a compromise between computational time and accuracy, we decided on an initial output time of 0.25 yr, which is small enough for these types of simulations (Horner et al. 2004a, 2004b), that would adjust itself to 0.01 yr during a close approach of a test particle to a planet during the time the test particle transformed into a JFC. An initial time step of 1 day was used for accuracy, which is less than one-thousandth the orbital period of Jupiter and is small enough to produce meaningful results (Nesvorný & Dones 2002; Tiscareno & Malhotra 2003; Horner et al. 2004a, 2004b; Roberts & Muñoz-Gutiérrez 2021). This time step adjusted itself to smaller values during a close approach of a test particle to a planet in order to maintain machine precision (Rein & Spiegel 2015). Though a close approach is said to occur whenever a small body

⁷ <https://mathworks.com/help/matlab/ref/matlab.graphics.chart.primitive.histogram.html> (Accessed: 2022 Feb. 7).

⁸ <https://ssd.jpl.nasa.gov/horizons/app.html/#/> (Accessed: 2021 Oct. 27).

approaches a planet within a distance of three Hill radii (Hsieh et al. 2020), we recorded the associated distance to Jupiter whenever a test particle evolved into a JFC.

The error in energy followed Brouwer’s law, which dictates that if the error is not due to systematic error and due only to random error in calculated values, using a limited number of decimal or bit places, then for an integration time, t_{int} , the error in energy grows with $t_{\text{int}}^{\frac{1}{2}}$, and the error in mean longitude of planets and small bodies grows with $t_{\text{int}}^{\frac{3}{2}}$ (Brouwer 1937).

We measured the fractional error in the energy of the system at each output time of 0.25 yr using

$$\frac{|E(t) - E(0)|}{E(0)}, \quad (7)$$

where $E(t)$ is the energy of the system at time t , and $E(0)$ is the energy of the system at $t = 0$. Our error analysis showed that the fractional error was on the order of 10^{-14} over 10^5 yr. In an analogous way, the fractional error in the total angular momentum of the system was found to be on the order of 10^{-14} .

To determine the positional errors of the planets, we integrated the planets forward for 10^5 yr and then backwards to $t = 0$. Then, at each output time of 0.25 yr, we calculated the absolute error between the mean longitude of each Jovian planet from the forward integration and the corresponding mean longitude from the backwards integration. The positional error was on the order of 10^{-8} radian for Jupiter, 10^{-8} radian for Saturn, 10^{-9} radian for Uranus, and 10^{-9} radian for Neptune.

Test particles were removed from the simulation upon colliding with a planet or the Sun (obtaining a heliocentric distance ≤ 0.005 au); obtaining a parabolic or hyperbolic orbit ($e \geq 1$); becoming a different type of SSSB such as a TNO ($a > 30.1$ au), an Encke-type comet ($Q < 4$ au, Horner et al. 2003), or a JFC and upon any close approach to Jupiter concluding; or obtaining a perihelion distance < 3 au for a time span of more than 20,000 yr (not necessarily consecutive).

This last condition was included because a typical JFC will lose its volatiles (fade) or disintegrate well before 20,000 yr (Whitman et al. 2006; Di Sisto et al. 2010) because water sublimation dominates the activity within a heliocentric distance of about 3.5 au (Whitman et al. 2006; Sarid et al. 2019).

3. Results

3.1. Overall Results

Out of the entire 22,625 test particles, 1725 (8%) survived for the entire integration time, 450 (2%) hit Jupiter, 38 (<1%) hit Saturn, 481 (2%) evolved into Encke-type comets, and 2352 (10%) became TNOs. We also found that 2685 test particles (12%) entered the outer main asteroid belt, defined using $2.8 \text{ au} < a < 3.2 \text{ au}$ (Farinella et al. 2001; Roig et al. 2002).⁹

We also checked for temporary satellite captures. A test particle was considered to be a temporary satellite of a planet if it entered the Hill sphere of the planet and the energy of the orbit of the test particle about the planet was negative (Carusi & Valsecchi 1983). We recorded 17,166 temporary satellite

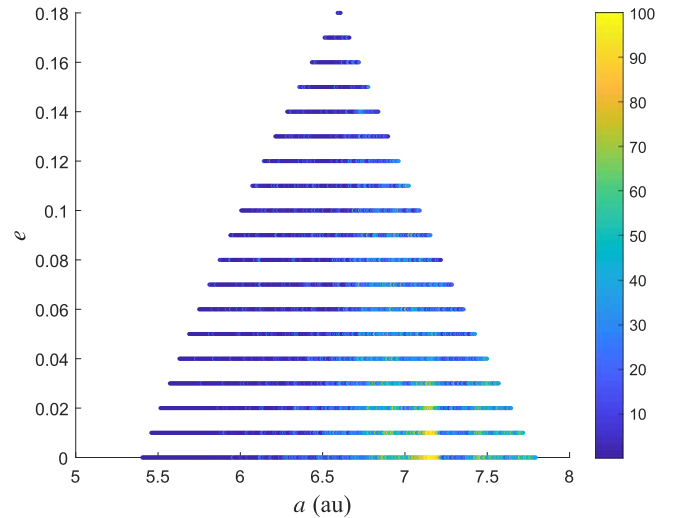


Figure 3. The initial semimajor axes and eccentricities of the orbits of test particles in $a - e$ space color-coded by dynamical lifetime in thousands of years. In general, those test particles with the smallest initial perihelion distances and semimajor axes evolved faster on average than those with the largest initial perihelion distances and semimajor axes.

captures (or TSCs) of 10,722 unique test particles (47%) into irregular satellite orbits.

Of these captures, 11,825 (69%) were with Jupiter and 5341 (31%) were with Saturn. The mean eccentricity of a test particle orbit at the start of a TSC was 0.87. Sometimes the life of a test particle would end during a TSC. For the 10,410 (61%) TSCs that were completed, the mean duration of capture was 6 yr. For 5634 TSCs (33%), the test particle started in a retrograde orbit relative to the equatorial plane. Satellites were determined to be irregular using the requirement of Burns & Matthews (1986), who stated that a satellite is irregular if the semimajor axis of its orbit about a planet is greater than a critical value, a_{crit} , given by

$$a_{\text{crit}} = \left(2J_2 r_p^2 a_p^3 \frac{M_p}{M_{\text{Sun}}} \right)^{\frac{1}{5}}, \quad (8)$$

where J_2 is the planet’s second gravitational harmonic coefficient and r_p is the equatorial radius of the planet. Using this formula with J_2 values given by Podolak & Helled (2012), we calculated a_{crit} to be $0.0437r_{\text{JH}}$, $0.0383r_{\text{SH}}$, $0.0193r_{\text{UH}}$, and $0.0156r_{\text{NH}}$ for Jupiter, Saturn, Uranus, and Neptune, respectively.

A total of 17,579, or 78%, of the test particles evolved into JFCs. This value is in good agreement with the value of 77% reported by Sarid et al. (2019) in their study. The mean time for a test particle to evolve into a JFC was 5808 yr, and the mean dynamical lifetime over all test particles was 16,811 yr. The median dynamical lifetime over all test particles was 1442 yr. The 16th percentile was 61 yr, and the 84th percentile was 38,074 yr.

Figure 3 shows the initial semimajor axes and eccentricities of the orbits of test particles in $a - e$ space color-coded by dynamical lifetime in thousands of years. In general, those test particles with the smallest initial perihelion distances and semimajor axes evolved faster on average than those with the largest initial perihelion distances and semimajor axes (Peixinho et al. 2020). For example, along a contour near

⁹ https://ssd.jpl.nasa.gov/tools/sbdb_query.html (Accessed: 2022 Feb. 8).

$q = 5.40$ au, the average dynamical lifetime was 8812 yr, while along a contour near $q = 7.06$ au it was 61,441 yr.

The mean time for a test particle to evolve into a JFC was 7475 yr. Positional errors in the planets did not exceed order 10^{-9} rad during this time interval. We found that a test particle evolved into a JFC via one of three different mechanisms. These were as follows:

1. Mechanism 1: the perihelion distance of the test particle's orbit abruptly, rapidly, and continually decreased until q became < 5.2 au, when its aphelion distance was already < 7 au. We will refer to this process as a JFC perihelion drop hereafter. We call the perihelion distance at the start and end of a drop q_{start} and q_{end} , respectively.
2. Mechanism 2: the aphelion distance of the test particle's orbit abruptly, rapidly, and continually decreased until Q became < 7 au, when its perihelion distance was already < 5.2 au. We will refer to this process as a JFC aphelion drop hereafter. We call the aphelion distance at the start and end of a drop Q_{start} and Q_{end} , respectively.
3. Mechanism 3: no drop was detected or $q_{\text{start}} - q_{\text{end}} < 0.001$ au for potential mechanism 1 drops or $Q_{\text{start}} - Q_{\text{end}} < 0.001$ au for potential mechanism 2 drops.

For mechanism 3, the distance 0.001 au was determined by trial and error. Of the test particles that evolved into a JFC, 9191 (41%) did so via a JFC perihelion drop, 8278 (37%) did so via a JFC aphelion drop, and 110 ($< 1\%$) did so via no drop. The average time for a test particle to become a JFC from the start of a JFC perihelion or aphelion drop was 4.7 yr and 1.7 yr, respectively. Of the 17,579 close approaches to Jupiter involved in the transformation of a test particle into a JFC, 1% were $< 0.01 r_{\text{JH}}$, 31% were $< 0.1 r_{\text{JH}}$, and 95% were $< 3 r_{\text{JH}}$.

To determine q_{start} and q_{end} for JFC perihelion drops, we started at the time the test particle became a JFC and then moved forward and backward in time, examining Δq , the change in q from one data point to the next ($\Delta q = q_{i+1} - q_i$ for the forward direction, and $\Delta q = q_i - q_{i+1}$ for the backward direction). After trial and error, we determined that a drop started and ended at a point where $|\Delta q|$ dropped below 0.001 au or Δq changed sign.

The process to find Q_{start} and Q_{end} for JFC aphelion drops was completely analogous. We discovered that JFC perihelion and aphelion drops were correlated with close approaches to Jupiter.

As an example, Figure 4 shows plots of the aphelion distance (green) and perihelion distance (blue) versus time, top panel, and the distance between the test particle and Jupiter, bottom panel, for a test particle that evolved into a JFC via a JFC perihelion drop during a time interval in which the test particle evolved into a JFC. In the top panel, the horizontal line is defined by $q = 5.2$ au. The sudden drop in perihelion distance starts at 23.25 yr. During the drop, the perihelion distance drops below 5.2 au, and the test particle becomes a JFC at 39.25 yr. In each plot, a magenta circle marks this point in time.

The drop ends at 44 yr. An asterisk marks q_{start} and q_{end} at 5.47 au and 5.07 au, respectively. The dynamical lifetime of this test particle is 44 yr, but it is integrated beyond this time so that the bottom of the drop can be clearly seen. In the bottom panel, the associated close approach to Jupiter occurs at a time of 38.5 yr at a distance of $5.17 r_{\text{JH}}$. A magenta circle marks this point in time.

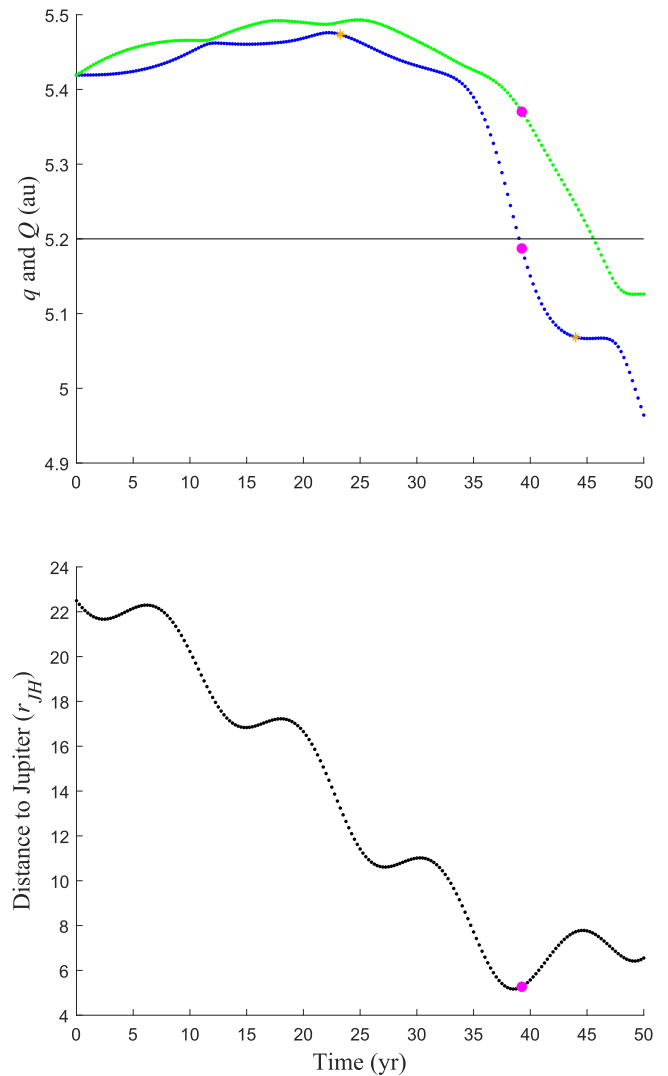


Figure 4. An example of a test particle that evolved into a JFC via a JFC perihelion drop. Top panel: the aphelion distance (green) and perihelion distance (blue) vs. time. The horizontal line is defined by $q = 5.2$ au. An asterisk marks q_{start} and q_{end} at 5.47 au and 5.07 au, respectively. Bottom panel: the distance between the test particle and Jupiter over the same time interval. A close approach to Jupiter occurs at a time of 38.5 yr at a distance of $5.17 r_{\text{JH}}$. The magenta circle in both panels marks the time when the test particle becomes a JFC.

Figure 5 shows analogous panels for a test particle that evolved into a JFC via a JFC aphelion drop during a time interval in which the test particle evolved into a JFC. In the top panel, the horizontal line is defined by $Q = 7$ au. The sudden drop in aphelion distance begins at 156.5 yr. During the drop, the aphelion distance drops below 7 au, and the test particle becomes a JFC at 159.5 yr. In each plot, a magenta circle marks this point in time.

The drop ends at 165 yr. An asterisk marks Q_{start} and Q_{end} at 9.31 au and 5.12 au, respectively. The dynamical lifetime of this test particle is 165 yr, but the test particle is integrated beyond this time so that the bottom of the drop can be clearly seen.

In the bottom panel, the associated close approach to Jupiter occurs at a time of 159.25 yr at a distance of $0.80 r_{\text{JH}}$. A magenta circle marks the time the test particle becomes a JFC.

To measure the severity of each JFC perihelion or aphelion drop, we calculated the fractional change in the associated

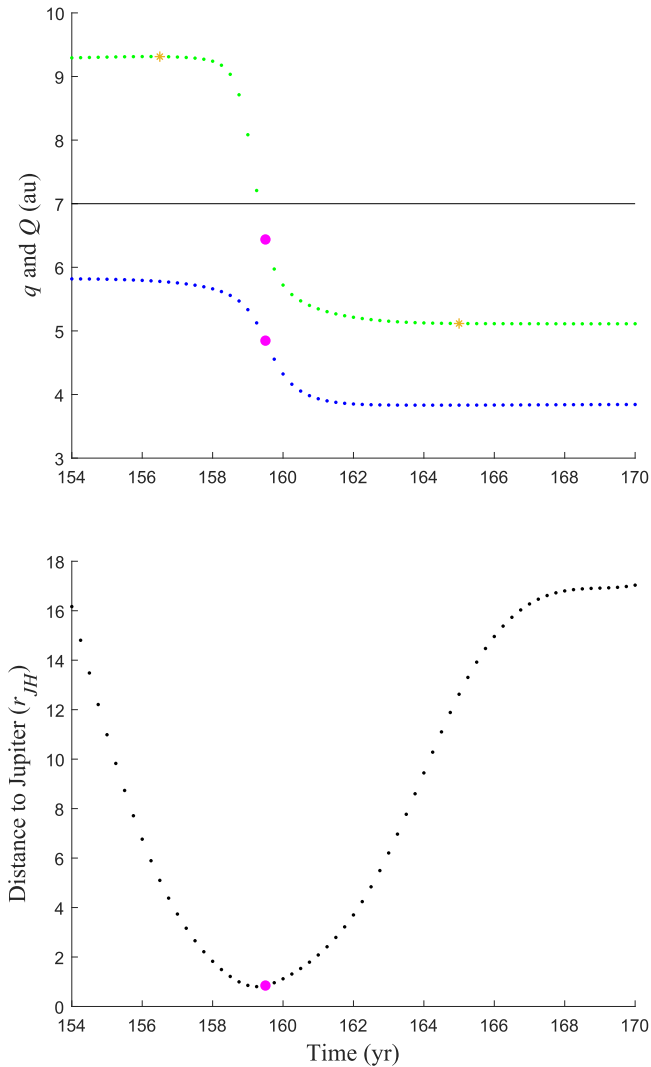


Figure 5. An example of a test particle that evolved into a JFC via a JFC aphelion drop. Top panel: the aphelion distance (green) and perihelion distance (blue) vs. time. The horizontal line is defined by $Q = 7$ au. An asterisk marks Q_{start} and Q_{end} at 9.31 au and 5.12 au, respectively. Bottom panel: the distance between the test particle and Jupiter over the same time interval. A close approach to Jupiter occurs at a time of 159.25 yr at a distance of $0.80r_{\text{JH}}$. The magenta circle in both panels marks the time when the test particle becomes a JFC.

perihelion or aphelion distance from the beginning to the end of the drop using an equation similar to Equation (7). For JFC perihelion drops, this equation is

$$\text{Severity} = \frac{q_{\text{start}} - q_{\text{end}}}{q_{\text{start}}}. \quad (9)$$

The equation for JFC aphelion drops is

$$\text{Severity} = \frac{Q_{\text{start}} - Q_{\text{end}}}{Q_{\text{start}}}. \quad (10)$$

The median severity over all drops was 0.41. The 16th percentile was 0.13, and the 84th percentile was 0.66. We analyzed our data by distributing all such drops into three distinct subsets: JFC aphelion drops, JFC perihelion drops with $Q < 7$ au at the start of the drop, and JFC perihelion drops with $Q \geq 7$ au at the start of the drop. For the first subset, interference from Saturn, Uranus, and Neptune is minimized

Table 1
Mean Inclinations

Subset	\bar{i}_{start} (deg.)	σ (deg.)
Q drops	4.29	4.99
q drops $Q < 7$ au	1.93	2.48
q drops $Q \geq 7$ au	2.27	2.84

Note. The mean inclination relative to the ecliptic plane and standard deviation, σ , at the start a JFC perihelion or aphelion drop for each subset of data.

so that the effect of Jupiter on each drop can be studied. Drops in the latter two subsets are affected by Jupiter but can also be influenced by Saturn, Uranus, and Neptune.

Table 1 shows the mean inclination relative to the ecliptic plane at the start of a JFC perihelion or aphelion drop for each subset, \bar{i}_{start} , along with its standard deviation, σ . Over all drops, the median inclination at the start of a drop was $1^{\circ}31'$. The 16th percentile was $1^{\circ}3'$, and the 84th percentile was $5^{\circ}14'$.

The mean inclination and its associated standard deviation relative to the ecliptic plane at the start a JFC perihelion or aphelion drop for each subset of data are shown in Table 1. The inclination of Jupiter's orbit is within one standard deviation of the mean inclination at the start of a JFC perihelion or aphelion drop. We consider these inclinations to be small enough and close enough to i_J so that any results based on values obtained at the start of a JFC perihelion or aphelion drop are an approximation to results that would be obtained in the planar problem with Jupiter.

3.2. JFC Perihelion Drops with $Q < 7$ au

A total of 5872 test particles evolved into JFCs via a JFC perihelion drop with $Q < 7$ au at the start of the drop. Figure 6 shows the time evolution of the perihelion distance of four test particles that became JFCs via a JFC perihelion drop with $Q < 7$ au at the start of the drop, during a time interval in which each test particle evolved into a JFC. The panels labeled (a), (b), (c), and (d) each represent one test particle. The severity of each drop is shown at the bottom of each panel. The horizontal line in each panel is defined by $q = 5.2$ au. The magenta circle in each panel marks the time when the test particle becomes a JFC. An asterisk marks q_{start} and q_{end} .

The close-approach distances to Jupiter for the test particles represented in panels (a), (b), (c), and (d) are $0.24r_{\text{JH}}$, $2.99r_{\text{JH}}$, $2.10r_{\text{JH}}$, and $5.82r_{\text{JH}}$, respectively. The corresponding values for q_{start} and q_{end} are 6.18 au, 5.29 au, 5.68 au, and 5.43 au; and 2.52 au, 4.55 au, 4.56 au, and 5.14 au. The corresponding dynamical lifetimes are 54.75 yr, 148.25 yr, 471.75 yr, and 44.25 yr.

The behavior of the Tisserand parameter with respect to Jupiter of the same four test particles over the same time intervals is shown in Figure 7, with panels that correspond to those in Figure 6. The horizontal line in each panel is defined by $T_J = 3$. The magenta circle in each panel marks the time when the test particle becomes a JFC. In each panel, T_J can be seen to drop below 3 as the test particle becomes a JFC. The severity of the drop is shown at the top center on each panel. A total of 530 T_J values at the start of a JFC perihelion drop in this subset were below 3 at the start of the drop.

Close-approach distances to Jupiter associated with each transformation into a JFC for this subset ranged from $0.0022r_{\text{JH}}$ to $27.9025r_{\text{JH}}$. The mean close-approach distance to Jupiter and

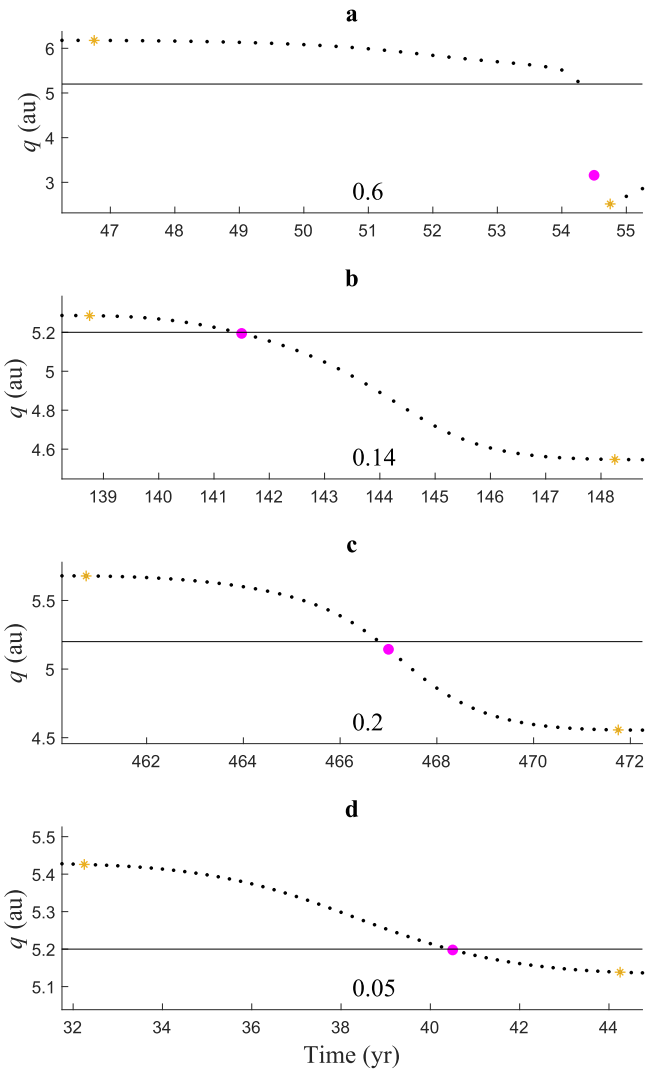


Figure 6. The time evolution of the perihelion distance of four test particles (one per panel) that became JFCs via a JFC perihelion drop with $Q < 7$ au at the start of the drop. The severity of each drop is shown at the bottom of each panel. The horizontal line in each panel is defined by $q = 5.2$ au. The magenta circle in each panel marks the time when the test particle becomes a JFC. An asterisk marks q_{start} and q_{end} .

its associated standard deviation for this subset were $1.08r_{\text{JH}}$ and $1.82r_{\text{JH}}$, respectively. Severities for this subset ranged from 0.0011 to 0.9998.

Figure 8 is a plot of the severity of the drop versus the \log_{10} of the close-approach distance to Jupiter in r_{JH} associated with the transformation into a JFC of test particles in this subset. For a given close-approach distance, there is a range of possible severities due to different relative velocities during the approach. But, in general, the smaller the close approach distance, the larger the maximum possible severity. This is because the closer the distance to Jupiter, the larger the potential gravitational perturbing force on q and thus the greater possible fractional change in q . The dashed vertical line represents a close-approach distance of $3r_{\text{JH}}$. Figure 9 shows a histogram of the \log_{10} of these same close-approach distances to Jupiter in r_{JH} . The distribution is double-peaked with peaks in the range $(-1.6, -1.4)$ and $(0.2, 0.4)$. The bin size is 0.2.

Figure 10 shows a histogram of the q_{start} values for this subset with a bin size of 0.05 au. A single peak is seen between 5.45 au and 5.50 au, and the count has a decreasing trend with

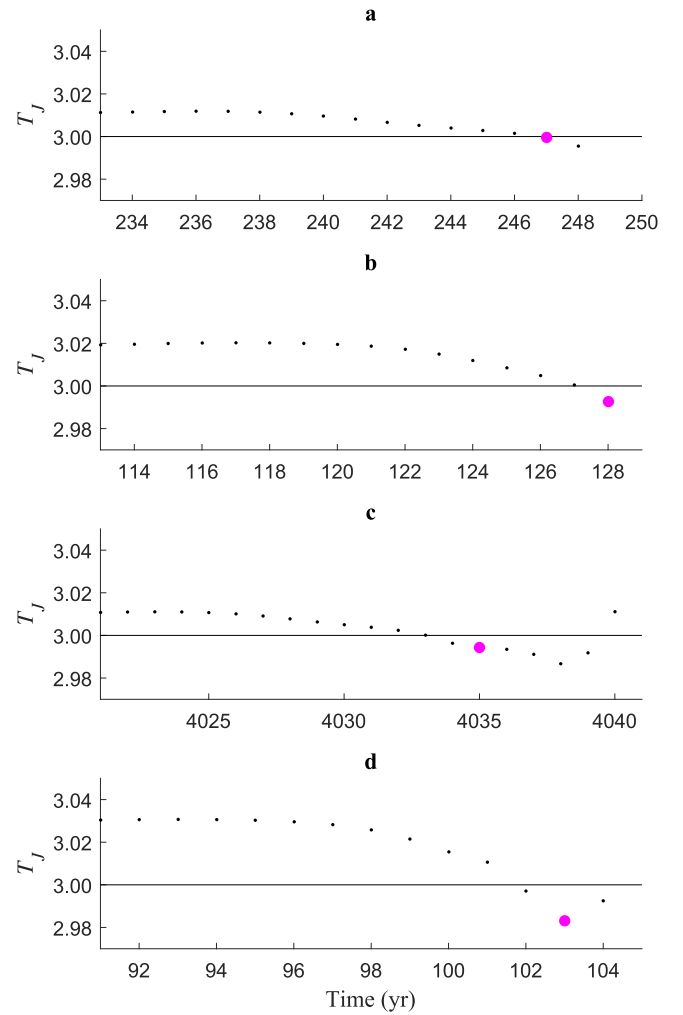


Figure 7. The Tisserand parameter with respect to Jupiter, T_J , of four test particles (one per panel) during a time interval in which each test particle evolved into a JFC via a JFC perihelion drop with $Q < 7$ au at the start of the drop. The magenta circle in each panel marks the time that the test particle becomes a JFC. The horizontal line in each panel is defined by $T_J = 3$. The severity of each drop is shown at the top center on each panel.

increasing q_{start} thereafter. The final bin is between 6.20 au and 6.25 au, and the largest q_{start} value recorded was 6.24 au. This is despite the fact that 39% of test particle orbits had an initial perihelion distance ≥ 6.3 au.

This suggests that 6.3 au is a perihelion barrier that must be crossed from above before a Centaur can evolve into a JFC due to a single close approach to Jupiter. Furthermore, if such a perihelion barrier is found in the planar problem with Jupiter, then the value of that barrier will also be the same in the nonplanar problem with Jupiter, since perturbing gravitational forces from Jupiter on perihelion distance are strongest in the planar problem (Murray & Dermott 1999). This means that changing the relative inclination, nodal distance (Saillenfest et al. 2017), and the MOID between the orbit of the test particle and the orbit of Jupiter will not raise the barrier above 6.3 au. That is, the perihelion distance barrier found in the planar problem with Jupiter is the barrier for all problems both planar and nonplanar, and our result is based on the approximate planar problem with Jupiter.

That is, given that all test particle orbits were initially coplanar with Jupiter's, if a single close encounter with Jupiter

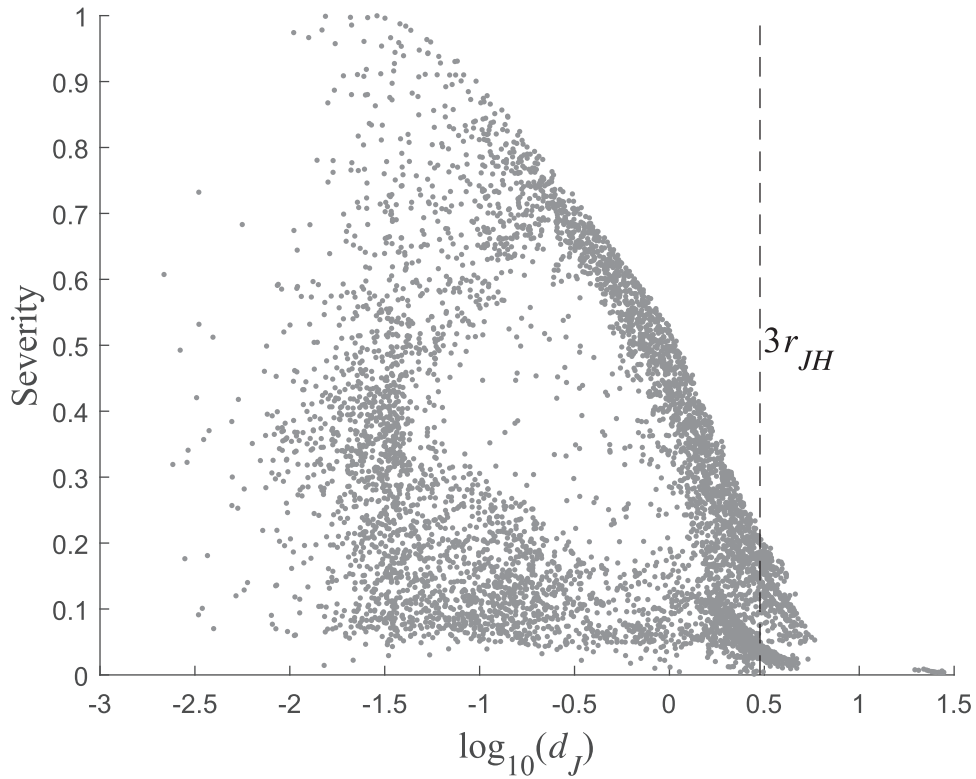


Figure 8. A plot of the severity of the drop vs. the \log_{10} of the close-approach distance to Jupiter associated with the transformation into a JFC of test particles that became JFCs via a JFC perihelion drop with $Q < 7$ au at the start of the drop. The dashed vertical line represents a close-approach distance of $3r_{JH}$. In general, the smaller the close-approach distance, the greater the maximum possible severity.

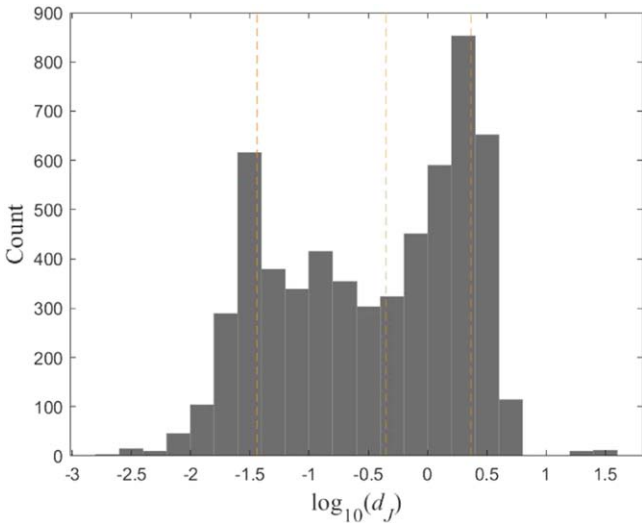


Figure 9. A histogram of the \log_{10} of close-approach distances to Jupiter in r_{JH} associated with the transformation into a JFC of the test particles that became a JFC via a JFC perihelion drop when $Q < 7$ au at the start of the drop. The distribution is double-peaked with peaks in the range $(-1.6, -1.4)$ and $(0.2, 0.4)$. The three dashed lines represent the 16th percentile, the median, and the 84th percentile, from left to right. The bin size is 0.2.

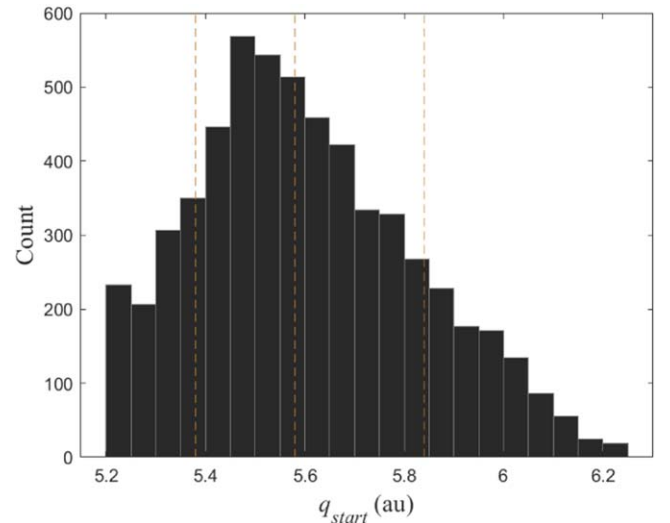


Figure 10. A histogram for the q_{start} values for JFC perihelion drops with $Q < 7$ au at the start of the drop. The bin size is 0.05 au. A single peak is seen between 5.45 au and 5.50 au. Distances are all below 6.3 au. The three dashed lines represent the 16th percentile, the median, and the 84th percentile, from left to right.

was capable of transforming a test particle into a JFC from an orbit with $q > 6.3$ au, then we would have expected to see this in our results.

We did find 20 test particles in this subset that had q_{start} values > 6.2 au in orbits coplanar with Jupiter's. Figure 11 shows a scatter plot of eccentricity versus semimajor axis for the known Centaurs as determined by the MPC and the known JFCs using the q-Q definition applied to the JPL Small-Body

Database. Centaurs are represented as dots and JFCs are represented as asterisks. A contour of constant perihelion distance of 6.3 au is also shown. As of this writing, 93 Centaurs (or 11%) have perihelion distances below 6.3 au and thus would be prone to JFC perihelion drops if 6.3 au is a perihelion barrier.

Using Equation (4), we calculated the critical inclination, i_{co} , relative to the ecliptic plane for which small bodies in orbits

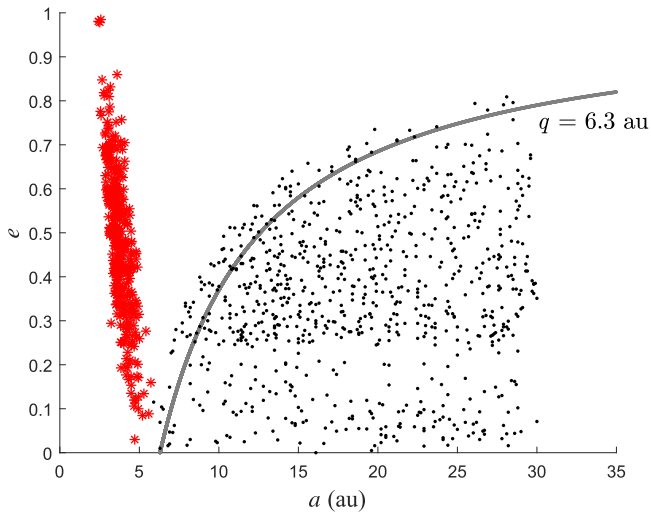


Figure 11. A scatter plot of eccentricity vs. semimajor axis for the known Centaurs as determined by the Minor Planet Center and the known JFCs using the q - Q definition applied to the JPL Small-Body Database. Centaurs are represented as dots and JFCs are represented as asterisks. A contour of constant perihelion distance of 6.3 au is also shown.

exterior to Jupiter with $i > i_{co}$ and $Q < 7$ au can have $q > 6.3$ au and $2 < T_J < 3$ but such orbits with $i \leq i_{co}$ cannot. i_{co} was found to be 10.2° .

Figure 12 shows the difference between orbits exterior to Jupiter with $i > i_{co}$ and such orbits with $i \leq i_{co}$. The figure shows contours defined by $T_J = 3$ in $q - Q$ space for orbits with inclinations of $i = 1.3^\circ$ (i_J), 6° , 8° , 10.2° , and 12° to the ecliptic plane in the ranges $5.1 \leq q \leq 7$ and $5.2 \leq Q \leq 7$. The two dashed vertical lines are defined by $q = 5.2$ au and $q = 6.3$ au.

Orbits in the shaded region with an inclination of 12° have $2 < T_J < 3$ and $q > 6.3$ au. Such regions also exist for other orbits with $i > i_{co}$ and have implications for comet taxonomy. Small bodies in the shaded region with an inclination of 12° would always be classified as JFCs using the taxonomical schemes of Levison (1996) and Di Sisto et al. (2019) but would be classified as Centaurs using the definition of the MPC. Furthermore, if 6.3 au is a perihelion barrier, then small bodies in the shaded region would not be subject to JFC perihelion drops. A total of 156 out of our examined 5872 test particles (2.66%) had an inclination above 10.2° at the start of a JFC perihelion drop.

3.3. JFC Aphelion Drops

A total of 8278 test particles became JFCs via a JFC aphelion drop. Severities for JFC aphelion drops ranged from 0.0730 to 0.9072. q values at the start of a JFC aphelion drop ranged from 0.54 au to 7.59 au, and Q_{start} values ranged from 7.00 au to 55.26 au. The mean time to transform into a JFC from the start of a JFC aphelion drop was 1.7 yr. Figure 13 shows a histogram of the \log_{10} of close-approach distances to Jupiter in r_{JH} associated with the transformation into a JFC of the test particles that became a JFC via a JFC aphelion drop. The bin size is 0.1. The distribution is double-peaked with peaks in the range $(-1.5, -1.4)$ and $(-0.5, -0.4)$. A total of 7304 T_J values were below 3 at the start of a JFC aphelion drop.

Figure 14 shows a plot of the severity of the drop versus the \log_{10} of the close-approach distance to Jupiter in r_{JH} associated

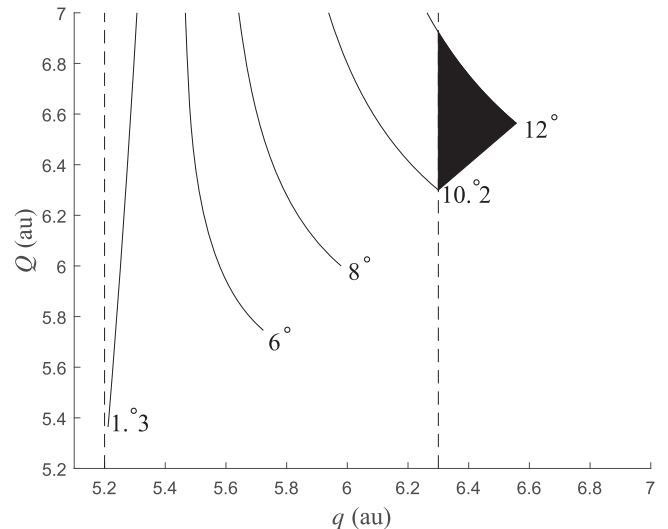


Figure 12. Contour curves defined by $T_J = 3$ in $q - Q$ space for inclinations of $i = 1.3^\circ$ (i_J), 6° , 8° , 10.2° , and 12° to the ecliptic plane. The two vertical lines are defined by $q = 5.2$ au and $q = 6.3$ au. In the shaded region, orbits with an inclination of 12° have $2 < T_J < 3$ and $q > 6.3$ au.

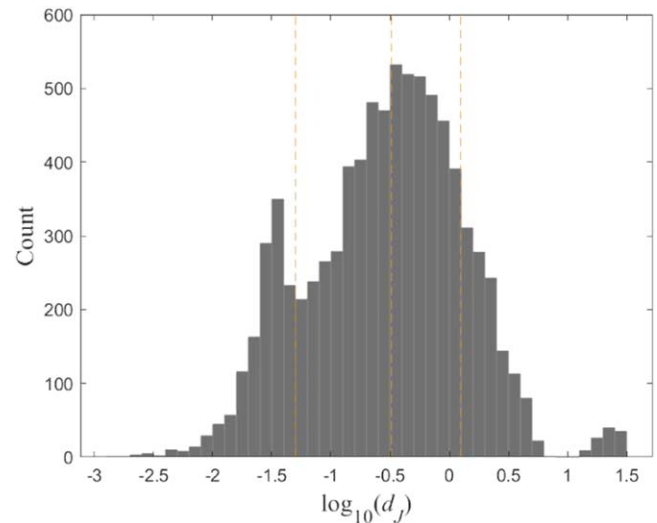


Figure 13. A histogram of the \log_{10} of close-approach distances to Jupiter in r_{JH} associated with the transformation into a JFC of the test particles that became a JFC via a JFC aphelion drop. The distribution is double-peaked with peaks in the range $(-1.5, -1.4)$ and $(-0.5, -0.4)$. The three dashed lines represent the 16th percentile, the median, and the 84th percentile, from left to right. The bin size is 0.1.

with the transformation of the test particles that became JFCs via a JFC aphelion drop. The data shows the same correlation between close-approach distance to Jupiter and maximum possible severity as was seen in Figure 8 for the previously discussed subset. That is, the smaller the close-approach distance, the larger the maximum possible severity. This suggests that Jupiter is still involved in the transformation of these test particles into JFCs. The mean close-approach distance to Jupiter and its associated standard deviation for this subset were $0.92r_{JH}$ and $2.68r_{JH}$, respectively. The dashed vertical line represents a close-approach distance of $3r_{JH}$.

Though Saturn could potentially influence all JFC aphelion drops, Uranus and Neptune could only influence drops for which $Q_{start} \geq q_{planet} - 3r_H$ or $a_{start} \geq q_{planet} - 4r_H$, where q_{planet} is the perihelion distance of a planet's orbit and a_{start}

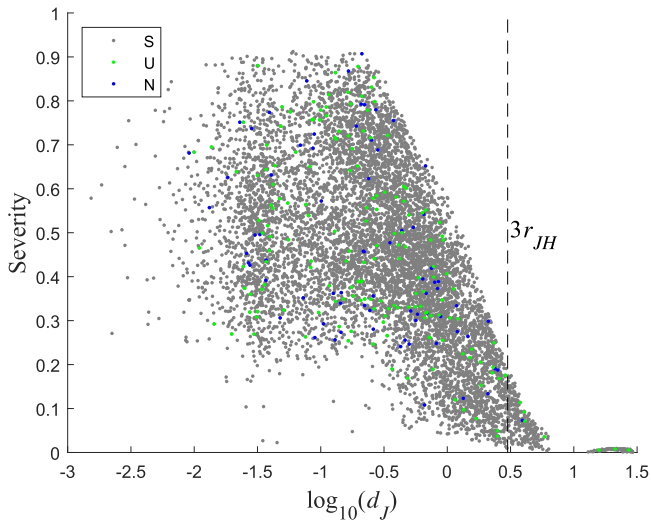


Figure 14. A plot of the severity of the drop vs. the \log_{10} of the close-approach distance to Jupiter in r_{JH} associated with the transformation into a JFC of the test particles that became JFCs via a JFC aphelion drop. The dashed vertical line represents a close-approach distance of $3r_{JH}$. Gray, green, and blue data points represent test particles whose transformation into a JFC could have been influenced by giant planets out to Saturn, Uranus, and Neptune, respectively.

is the semimajor axis of the orbit of a test particle at the start of a drop (Sarid et al. 2019).

Using these formulae, we detected potential influence by Uranus on the JFC aphelion drop of 169 test particles and by Neptune on the JFC aphelion drop of 74 test particles in this subset. Gray, green, and blue data points represent test particles whose transformation into a JFC could have been influenced by giant planets out to Saturn, Uranus, and Neptune, respectively.

3.4. JFC Perihelion Drops with $Q \geq 7$ au

A total of 3319 test particles became JFCs via a JFC perihelion drop with $Q \geq 7$ au at the start of the drop. q_{start} values for this subset ranged from 5.2 au to 6.9 au, and the mean time to transform into a JFC from the start of a drop was 3.7 yr. Figure 15 shows a histogram of the q_{start} values for this subset. The bin size is 0.05 au. The distribution is double-peaked with peaks in the ranges (5.4 au, 5.45 au) and (5.85 au, 5.9 au). Above 5.9 au, the count has a decreasing trend with increasing q_{start} until the count drops to zero between 6.25 au and 6.35 au.

Nine drops had $q_{\text{start}} \geq 6.3$ au. We were able to correlate the transformation into a JFC of each of these nine test particles with close approaches to Saturn within four Saturn Hill radii. For each of these nine cases, a close approach to Saturn caused the perihelion distance to drop below 6.3 au after the JFC perihelion drop began. Then, a close approach to Jupiter dropped the perihelion distance below 5.2 au.

Figure 16 shows an example of this. The top panel shows the perihelion distance (blue) and aphelion distance (green) of a test particle over a time interval during which the test particle becomes a JFC. The magenta circle in each panel marks the time the test particle becomes a JFC. The orange asterisks are at the times of q_{start} and q_{end} . The red asterisk is at the time of close approach to Saturn, and the red diamond is at the time of close approach to Jupiter.

The JFC perihelion drop begins at 585.25 yr when $q = 6.394$ au, and the test particle is already on its way to a close approach to Saturn. At 588.5 yr q drops below 6.3 au, and

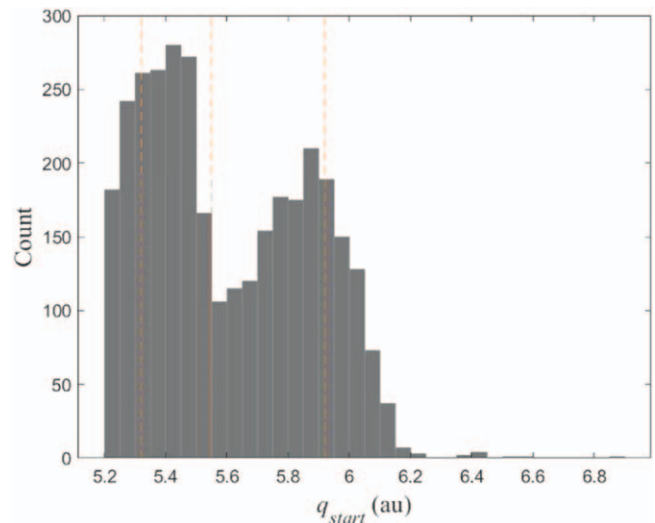


Figure 15. A histogram for the q_{start} values for JFC perihelion drops with $Q \geq 7$ au at the start of the drop. The three dashed lines represent the 16th percentile, the median, and the 84th percentile, from left to right. The bin size is 0.05 au. The distribution is double-peaked with peaks in the ranges (5.4 au, 5.45 au) and (5.85 au, 5.9 au). Values of $q_{\text{start}} \geq 6.3$ au can be explained by close approaches to Saturn.

at 591.5 yr the test particle experiences a close approach to Saturn at a distance of $1.62r_{SH}$. At 600 yr the test particle experiences a close approach to Jupiter at a distance of $1.45r_{JH}$ and transforms into a JFC at 600.5 yr. The drop ends at 607.25 yr when $q = 4.079$ au. The dynamical lifetime of this test particle is 607.25 yr.

The middle panel shows the distance between the test particle and Saturn versus time over the same time interval as that of the top panel. The red asterisk is at the time of close approach to Saturn. The bottom panel shows the distance between the test particle and Jupiter versus time over the same time interval as that of the top panel. The red diamond is at the time of close approach to Jupiter. Thus, this data agrees with our previous result that 6.3 au is a perihelion barrier that must be crossed from above before a single close approach to Jupiter alone can transform a Centaur into a JFC.

Figure 17 shows a histogram of the \log_{10} of the close-approach distances to Jupiter in r_{JH} associated with the transformation into a JFC of the test particles in this subset. The bin size is 0.2. The distribution is double-peaked with peaks in the range $(-1.6, -1.4)$ and $(-0.2, 0)$. The mean close-approach distance to Jupiter and its associated standard deviation for this subset were $0.43r_{JH}$ and $1.05r_{JH}$, respectively.

Figure 18 shows a plot of the severity of the drop versus the \log_{10} of the close-approach distance to Jupiter in r_{JH} associated with the transformation into a JFC of the test particles in this subset. Severities ranged from 0.0127 to 0.9022. The dashed vertical line represents a close-approach distance of $3r_{JH}$.

Using the previously described method for each planet, we detected potential influence by Uranus on the JFC perihelion drop of 31 test particles and by Neptune on the JFC perihelion drop of 16 test particles in this subset. Gray, green, and blue data points represent test particles whose transformation into a JFC could have been influenced by giant planets out to Saturn, Uranus, and Neptune, respectively.

Q values at the start of a JFC perihelion drop for this subset ranged from 7.0 au to 54.4 au. A total of 1449 T_J values at the

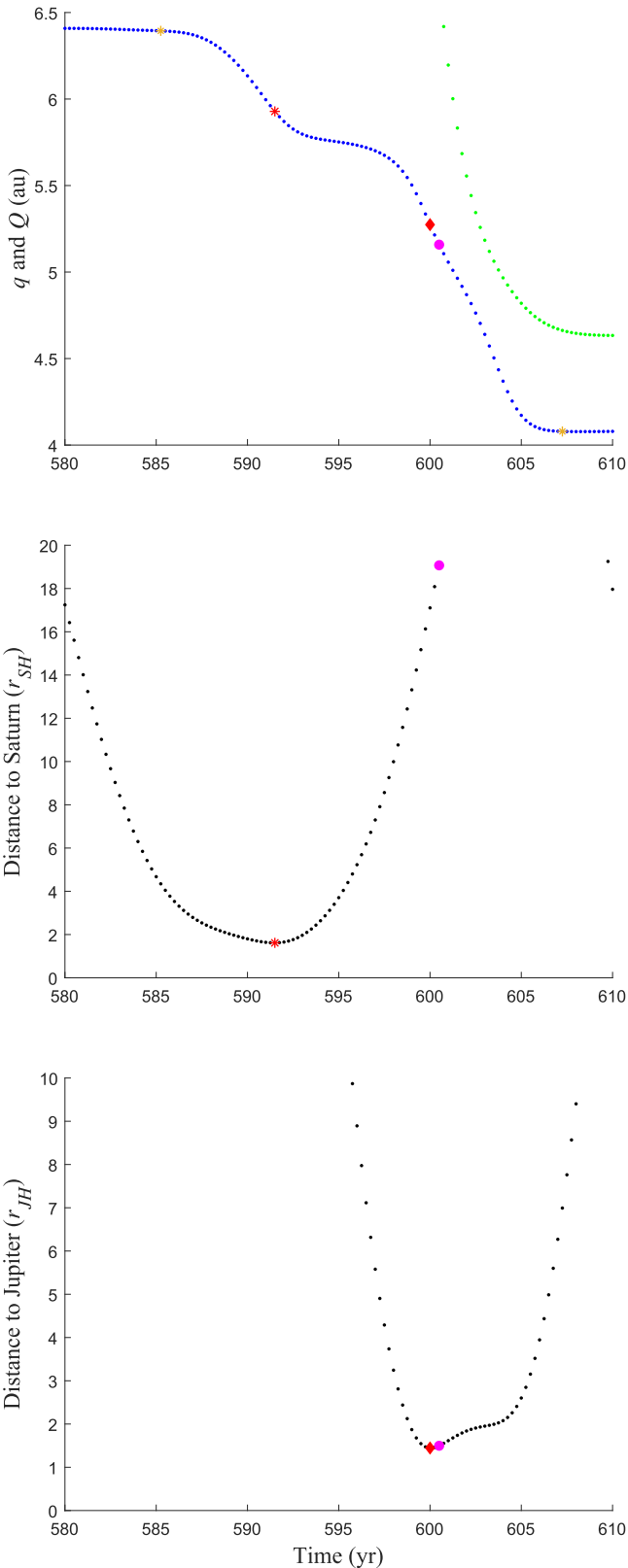


Figure 16. Top panel: the perihelion distance (blue) and aphelion distance (green) of a test particle over a time interval during which the test particle becomes a JFC via a JFC perihelion drop. Middle panel: the distance between the test particle and Saturn vs. time over the same time interval. Bottom panel: the distance between the test particle and Jupiter vs. time over the same time interval. The orange asterisks are at the times of q_{start} and q_{end} . The red asterisk is at the time of close approach to Saturn. The red diamond is at the time of close approach to Jupiter. The magenta circle in each panel marks the time the test particle becomes a JFC.

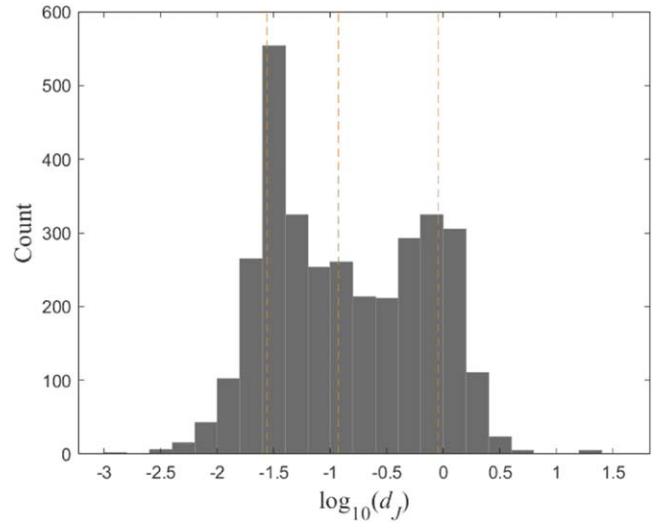


Figure 17. A histogram of the \log_{10} of close-approach distances to Jupiter in r_{JH} associated with the transformation into a JFC of the test particles that became a JFC via a JFC perihelion drop with $Q \geq 7$ au at the start of the drop. The three dashed lines represent the 16th percentile, the median, and the 84th percentile, from left to right. The bin size is 0.2. The distribution is double-peaked with peaks in the range $(-1.6, -1.4)$ and $(-0.2, 0)$.

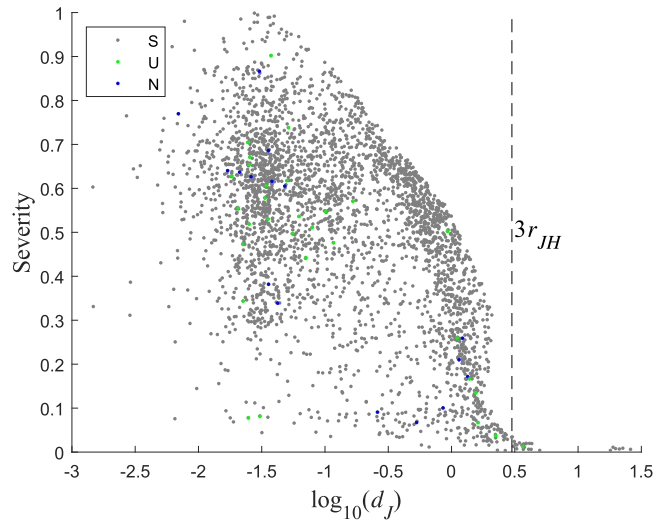


Figure 18. A plot of the severity of the drop vs. the \log_{10} of the close-approach distance to Jupiter in r_{JH} associated with the transformation into a JFC of each test particle that became a JFC via a JFC perihelion drop with $Q \geq 7$ au at the start of the drop. The dashed vertical line represents a close-approach distance of $3r_{JH}$. Gray, green, and blue data points represent test particles whose transformation into a JFC could have been influenced by giant planets out to Saturn, Uranus, and Neptune, respectively.

start of a JFC perihelion drop in this subset were below 3 at the start of the drop.

4. Conclusions

It is well known that Centaurs can evolve into JFCs over time due to gravitational perturbations from the giant planets. But since there is no universally accepted definition of a JFC, the exact point in time at which a Centaur transforms into a JFC can be debatable. JFCs are loosely defined as short-period comets with orbital periods < 20 yr whose dynamics are mainly controlled by Jupiter (Marsden 2009).

We adopted the q-Q definition in which a small body is considered to be a JFC if $2 < T_J < 3$, its perihelion distance, q , is $q < a_J$, and its aphelion distance, Q , is $Q < 7$ au where $a_J = 5.2$ au, the semimajor axis of Jupiter.

In this work, we studied the transformation of Centaurs into JFCs using the technique of numerical integration of 22,625 massless test particles in the six-body problem (the Sun, four giant planets, and a test particle).

In general, test particles in orbits with the smallest perihelion distances and semimajor axes evolved the fastest on average. The mean time for a test particle to evolve into a JFC was 5808 yr, and the mean dynamical lifetime over all test particles was 16,811 yr.

Test particles evolved into JFCs via one of three mechanisms: by a continuous drop in perihelion distance in which q dropped below a_J , by a continuous drop in aphelion distance in which Q dropped below 7 au, or by no drop (or negligible drop) in q or Q . We referred to the former two drops as JFC perihelion drops and JFC aphelion drops, respectively, and restricted our study to those.

Out of the entire 22,625 test particles, 2% became Encke-type comets, 10% became TNOs, 47% became irregular temporary satellites of either Jupiter or Saturn at least once, 12% entered the outer main asteroid belt, and 78% evolved into JFCs, 41% via a JFC perihelion drop and 37% via a JFC aphelion drop. Only <1% did so via no drop. Test particles transformed into JFCs via an aphelion or perihelion drop on average within 5 yr from the start of the drop.

Both JFC perihelion and aphelion drops were correlated with a close approach of a test particle to Jupiter. Though Saturn, Uranus, and Neptune could have potentially influenced drops with $Q \geq 7$ au at the start of the drop, close approaches to Jupiter were still strongly involved in the transformation process.

We measured the severity of JFC perihelion and aphelion drops by calculating the fractional change in the associated perihelion or aphelion distance due to the drop. The severities ranged from 0.0007 to 0.9998. In general, the smaller the close-approach distance, the larger the maximum possible severity of the drop.

JFC perihelion drops due solely to a close approach to Jupiter always commenced when $q_{\text{start}} < 6.3$ au, where q_{start} was the value of q at the start of the drop. This value was found approximately for the planar problem. Since only planar perturbing gravitational forces from Jupiter can change q , the value of 6.3 au should be independent of inclination and nodal distance. Thus, 6.3 au may be a perihelion barrier that must be crossed from above in order for a Centaur to transform into a JFC due to a single close approach to Jupiter. Only 93 (or 11%) of the currently known Centaurs have a perihelion distance below 6.3 au.

If the inclination of the orbit of the Centaur to the ecliptic plane is above $10^\circ.2$ then orbits with $q > 6.3$ au and $2 < T_J < 3$ can exist. Small bodies in such regions with $i > i_{\text{co}}$ would not be prone to JFC perihelion drops if 6.3 au is a perihelion barrier and could be classified as JFCs or Centaurs depending on the taxonomical scheme used.

T.C.H. acknowledges financial support from the National Research Foundation (NRF), grant No. 2019R111A1A01059609. We would like to thank the anonymous referee for their valuable feedback.

This research has made use of data and/or services provided by the International Astronomical Union's Minor Planet Center, NASA, and the Jet Propulsion Laboratory.

ORCID iDs

Jeremy Wood  <https://orcid.org/0000-0003-1584-302X>
Tobias C. Hinse  <https://orcid.org/0000-0001-8870-3146>

References

- Bailey, B. L., & Malhotra, R. 2009, *Icar*, **203**, 155
 Brassier, R., Schwamb, M. E., Lykawka, P. S., & Gomes, R. S. 2012, *MNRAS*, **420**, 3396
 Brouwer, D. 1937, *AJ*, **46**, 149
 Burns, J. A., & Matthews, M. S. 1986, Satellites (Tucson, AZ: Univ. of Arizona Press), 1032, For individual items see A87-23308 to A87-23325
 Carusi, A., & Valsecchi, G. B. 1983, Asteroids, Comets, and Meteors (Uppsala, Sweden: Astronomiska Observatoriet), 331
 de la Fuente Marcos, C., & de la Fuente Marcos, R. 2014, *Ap&SS*, **352**, 409
 Di Sisto, R. P., & Brunini, A. 2007, *Icar*, **190**, 224
 Di Sisto, R. P., Fernández, J. A., & Brunini, A. 2010, IAU Symp. 263, Icy Bodies of the Solar System (Cambridge: Cambridge Univ. Press), 102
 Di Sisto, R. P., Ramos, X. S., & Gallardo, T. 2019, *Icar*, **319**, 828
 Dones, L., Levison, H. F., & Duncan, M. J. 1996, in ASP Conf. Ser. 107, Completing the Inventory of the Solar System, ed. T. W. Rettig & J. M. Hahn (San Francisco, CA: ASP), 233
 Duncan, M., Levison, H., & Dones, L. 2004, Dynamical Evolution of Ecliptic Comets. In Comets II (M. Festou et al., eds.), This Volume (Tucson: Univ. Arizona)
 Emel'yanenko, V. V., Asher, D. J., & Bailey, M. E. 2005, *MNRAS*, **361**, 1345
 Farinella, P., Foschini, L., Froeschlé, C., et al. 2001, *A&A*, **377**, 1081
 Fernández, J. A., Helal, M., & Gallardo, T. 2018, *P&SS*, **158**, 6
 Fouchard, M., Rickman, H., Froeschlé, C., & Valsecchi, G. B. 2014, *Icar*, **231**, 99
 Grazier, K. R. 2016, *AsBio*, **16**, 23
 Grazier, K. R., Horner, J., & Castillo-Rogez, J. C. 2019, *MNRAS*, **490**, 4388
 Gkotsinas, A., Guilbert-Lepoutre, A., Raymond, S. N., & Nesvorný, D. 2022, *ApJ*, **928**, 43
 Hahn, G., & Bailey, M. E. 1990, *Natur*, **348**, 132
 Horner, J., Evans, N. W., Bailey, M. E., & Asher, D. J. 2003, *MNRAS*, **343**, 1057
 Horner, J., Evans, N. W., & Bailey, M. E. 2004a, *MNRAS*, **355**, 798
 Horner, J., Evans, N. W., & Bailey, M. E. 2004b, *MNRAS*, **354**, 798
 Horner, J., & Jones, B. W. 2009, *IJAsB*, **8**, 75
 Horner, J., & Lykawka, P. S. 2010, *MNRAS*, **402**, 13
 Horner, J., Lykawka, P. S., Bannister, M. T., & Francis, P. 2012, *MNRAS*, **422**, 2145
 Horner, J., Müller, T. G., & Lykawka, P. S. 2012, *MNRAS*, **423**, 2587
 Horner, J., & Wyn Evans, N. 2006, *MNRAS*, **367**, L20
 Hsieh, H. H., Novaković, B., Walsh, K. J., & Schörghofer, N. 2020, *AJ*, **159**, 179
 Jehin, E., Manfroid, J., Hutsemékers, D., et al. 2006, *ApJL*, **641**, L145
 Jewitt, D. 2009, *AJ*, **137**, 4296
 Levison, H. F. 1996, in ASP Conf. Ser. 107, Completing the Inventory of the Solar System, ed. T. W. Rettig & J. M. Hahn (San Francisco, CA: ASP), 173
 Levison, H. F., & Duncan, M. J. 1994, *Icar*, **108**, 18
 Levison, H. F., & Duncan, M. J. 1997, *Icar*, **127**, 13
 Lykawka, P. S., & Horner, J. 2010, *MNRAS*, **405**, 1375
 Marsden, B. G. 2009, *P&SS*, **57**, 1098
 MATLAB 2018, MATLAB version 9.4.0.949201 R2018a (Natick, MA: The Mathworks, Inc.)
 Murray, C. D., & Dermott, S. F. 1999, Solar System Dynamics (Cambridge: Cambridge Univ. Press)
 Nesvorný, D., & Dones, L. 2002, *Icar*, **160**, 271
 Park, R. S., Folkner, W. M., Williams, J. G., & Boggs, D. H. 2021, *AJ*, **161**, 105
 Peixinho, N., Thirouin, A., Tegler, S. C., et al. 2020, The Trans-Neptunian Solar System (Amsterdam: Elsevier), 307
 Podolak, M., & Helled, R. 2012, *ApJL*, **759**, L32
 Rein, H., & Liu, S.-F. 2012, *A&A*, **537**, A128
 Rein, H., & Spiegel, D. S. 2015, *MNRAS*, **446**, 1424
 Roberts, A. C., & Muñoz-Gutiérrez, M. A. 2021, *Icar*, **358**, 114201

- Roig, F., Nesvorný, D., & Ferraz-Mello, S. 2002, *MNRAS*, **335**, 417
- Saillenfest, M., Fouchard, M., Tommei, G., & Valsecchi, G. B. 2017, *CeMDA*, **129**, 329
- Sarid, G., Volk, K., Steckloff, J. K., et al. 2019, *ApJL*, **883**, L25
- Sellers, J. J., Astore, W. J., Griffen, R. B., & Larson, W. J. 2005, *Understanding Space: An Introduction to Astronautics* (3rd ed.) (New York: McGraw Hill, Inc.)
- Stodolna, J., Gainsforth, Z., Butterworth, A. L., & Westphal, A. J. 2014, *E&PSL*, **388**, 367
- Tiscareno, M., & Malhotra, R. 2003, *AJ*, **126**, 3122
- Volk, K., & Malhotra, R. 2008, *ApJ*, **687**, 714
- Whitman, K., Morbidelli, A., & Jedicke, R. 2006, *Icar*, **183**, 101
- Wiźniowski, T., & Rickman, H. 2013, *AcA*, **63**, 293
- Wood, J. 2019, *The Dynamics of Small Solar System Bodies*, SpringerBriefs in Astronomy (Switzerland: The Author(s), under exclusive license to Springer Nature)
- Wood, J., Horner, J., Hinse, T. C., & Marsden, S. C. 2017, *AJ*, **153**, 245
- Wood, J., Horner, J., Hinse, T. C., & Marsden, S. C. 2018a, *AJ*, **155**, 2
- Wood, J., Horner, J., Hinse, T. C., & Marsden, S. C. 2018b, *MNRAS*, **480**, 4183